Hindawi
Geofluids
Volume 2022, Article ID 5924648, 15 pages
https://doi.org/10.1155/2022/5924648

Research Article

Seismic Performance of a New Slurry-Anchored Connected Precast Concrete Shear Walls with Vertical Reinforcement

Yuqi Liu, Quandong Xiao, and Xingwen Yin

College of Civil Engineering, Hunan University of Science and Technology, Xiangtan 411201, China

Correspondence should be addressed to Yuqi Liu; lyq690893172@163.com

Received 21 January 2022; Revised 14 March 2022; Accepted 21 March 2022; Published 21 April 2022

Academic Editor: Yi Liu

The effectiveness of joint connection mode of PC shear wall structure directly determines the integrity and seismic performance of the structure. In this paper, a new type of grout-anchor connection of PC shear wall with closed stirrup constraint is proposed. For the investigation of the seismic performance of these shear walls, one cast-in-place shear wall specimen and two new slurry-anchored lap PC shear wall specimens were subjected to quasistatic test. The experimental results were verified and parametrically analyzed using the ABAQUS software. The test results showed that the slurry-anchored connection with buckled closed stirrups restraint could effectively transfer the stress. The PC shear walls and cast-in-place shear walls exhibited similar seismic performance and both exhibited bending shear damage when damaged. In general, the PC shear walls had a stronger bearing capacity and better displacement ductility performance than cast-in-place shear walls. Their energy dissipation capacity was similar to that of cast-in-place shear walls, but their initial stiffness was lower than that of cast-in-place shear walls. The numerical simulation results showed that, by increasing the axial compression ratio, the vertical connection reinforcement diameter, and the concrete strength, the stiffness and the load-carrying capacity of the horizontally jointed assembled shear wall structure could be improved within a certain range. With an increase in the height-to-width ratio, the peak load of the PC shear wall model decreased, while the ductility and the energy dissipation capacity were enhanced.

1. Introduction

Precast concrete (PC) shear wall structure has been rapidly developed and widely used in recent years to meet the structural performance requirement for high-rise housing buildings in line with the development trend of industrialization of the construction industry [1–3]. As an important connection part in PC shear wall structures, the effectiveness of the horizontal and vertical joints directly determines the integrity and the seismic performance of the structure. In recent years, to improve the seismic performance of PC shear walls with horizontal joints, scholars have conducted a lot of researches on the design of structural details and new connections in PC shear walls [4–6]. The connections of horizontal joints in PC shear wall structures can be divided into dry connections and wet connections.

Dry connections in PC shear wall structures include bolted connections and unbonded prestressed connections. Sun et al. [7–9] proposed the use of dry connection through a horizontal steel connector and high-strength bolts for PC shear walls. The experimental results showed that the PC shear wall joined by bolted connections under monotonic and cyclic loadings had good energy dissipation capacity and ductility. Wanrun [10] developed a new bolt-plate connection joint assembled by the high-strength bolt with an embedded steel plate in the PC shear wall. They conducted an experimental investigation to find that the damage pattern of the prestressed concrete wall with bolt-plate connection was similar to that of the cast-in-place shear wall. Bolt-plate connection joint could effectively improve the plastic deformation capacity of the PC shear wall. In recent years, unbonded prestressed connections have received attention from a wide range of scholars due to their good seismic performance. Research results have shown that post-tensioned prestressed PC shear walls have a strong self-resetting capability and minimal structural damage. They can reduce the residual displacement of PC shear walls

[11–13], but the engineering economy of this method is low [14].

For wet connections of PC shear walls, the members are generally connected using grout or cast-in-place concrete including metal bellows connections and sleeve grout connections. Sleeve grouting connections have been widely used in Asia, Europe, and America due to their advantages such as the good economy and ease of construction. Min et al. [15] studied the seismic performance of PC short-limb shear walls connected by sleeve grouting and showed that the ductility and the energy dissipation capacity of the PC shear wall specimens were lower than those of the cast-in-place specimens and the connection failure between the grout and the vertically connected reinforcement in the sleeve occurred after the specimens yielded. Zhi et al. [16] conducted an experimental study on four different reinforcements of PC shear walls connected by metal bellows slurry-anchored under low circumferential repeated loads. This study showed that PC shear walls connected by metal bellows had a better seismic performance. It was also shown that the load-bearing capacity of PC shear walls connected by metal bellows using high-strength reinforcement was greater. In the past occurrence of earthquakes, it could be found that poor structural design was one of the reasons for the inadequate seismic performance of PC shear wall specimens [17–20]. To improve the seismic performance of PC shear walls, scholars have studied the seismic performance of PC shear walls under different lap joint methods. Li et al. [21] and Xue et al. [22] both used two layers of pinned reinforcement with different lap lengths such as staggered laps to reduce the lap rate of the section of reinforcement. The results of both of these studies showed the effectiveness of staggered laps for vertical reinforcement. Among the existing vertical reinforcement lap joint methods for PC shear walls, the stirrup connection has a shorter lap length with a higher tolerance. According to the existing codes [23–26], the lap length can be reduced to 50-70% of that for the straight rebar. Jiang et al. [27] designed a PC shear wall with two different vertical reinforcement connections (ordinary stirrups and spiral stirrups) and found that the bearing capacity of the PC shear wall specimen was slightly lower than that of the cast-in-place shear wall specimen. However, its ductility was significantly higher than that of the cast-in-place shear wall specimen according to the comparison tests. Jiao et al. [28] studied and tested 15 shear wall specimens under the influence of different connection forms, steel configurations, axial compression ratios, and other parameters. Their results showed that the shear wall specimens with ring bar buckling anchor connection had a good seismic performance. The load-bearing capacity, the energy dissipation, and the ductility of stirrup-encrypted PC shear wall specimens were the same as those of fully PC specimens. Rossley et al. [29] proposed a loop bars connection for PC shear walls, and they found that this connection showed ductile behavior by producing a few line cracks and having a large deflection to give warning before failure.

At present, the restraint method of PC shear wall grout anchor to connect vertical steel bars has a certain restraint effect, but the actual construction is complicated, and the effect of popularization and use is not positive. Compared with the existing restraint methods, the construction and operation of the joint closure stirrups is less difficult and the amount of steel used is less; therefore, it is proposed that the use of joint closure stirrups should be used to restrain the vertical reinforcement. For investigating the effect of joint closure stirrups on the seismic performance of this structure, quasistatic test on one cast-in-place shear wall specimen and two new slurry-anchored connected PC shear wall specimens was conducted. The corresponding finite element models were also established to further explore the influences of the axial compression ratio, the height-to-width ratio, the longitudinal connection reinforcement diameter, and the concrete strength on the seismic performance of the new slurry-anchored connected PC shear wall with horizontal joints. Some suggestions were also made for the further research and application of this PC shear wall structure.

2. Test Specimens and Program

2.1. Design of the Specimens. A total of three full-scale wall specimens of the same size and reinforcement were designed according to the Chinese Code for Seismic Design of Buildings (GB50011-2010) [30] and Chinese PC concrete structure codes (GB51231-2016) under the force-based design [31], including one cast-in-place specimen CW1 and two assembled shear wall specimens FW1 and FW2; the dimensions and reinforcement details of the three specimens are shown in Figure 1. The PC specimens FW1, FW2 are preburied with 40 mm metal bellows, and thefastener closure stirrups are located under the constraint of vertical steelbars at the dark columns at both ends of the PC shear wall. Three horizontalfastener closure stirrups are set on each side of the same height, the laplength to the steel bar is 600mm.

The concrete design strength grade of the three shear wall walls in the test is C35, and the postcast part of the PC shear wall specimen is made of high-strength nonshrink cement-based grout, and the measured values of the concrete mechanical properties are shown in Table 1, and steel material performance measured values are shown in Table 2.

2.2. Fabrication of Specimen. The shear wall specimens are made according to the actual engineering construction technology; the cast-in-place shear wall, the base, and the loading beam are cast as a whole by the template; the PC shear wall and the base are made separately. Vertical reinforcement should be reserved for the base of prefabricated shear wall, and 20 mm slurry layer should be set up. The vertical reinforcement connection at the connection is restrained by buckle-closed stirrups. The PC shear wall loading beam and the wall are grouted in the metal bellows. The assembled prefabricated specimens are shown in Figure 2.

2.3. Test Setup and Loading Process. The low-cycle repeated load test is used to simulate the stress and deformation performance of the structure in the reciprocating vibration during earthquake. The test loading device consists of horizontal and vertical devices, as shown in Figure 3. The vertical load is provided by the piercing jack, and the test piece is

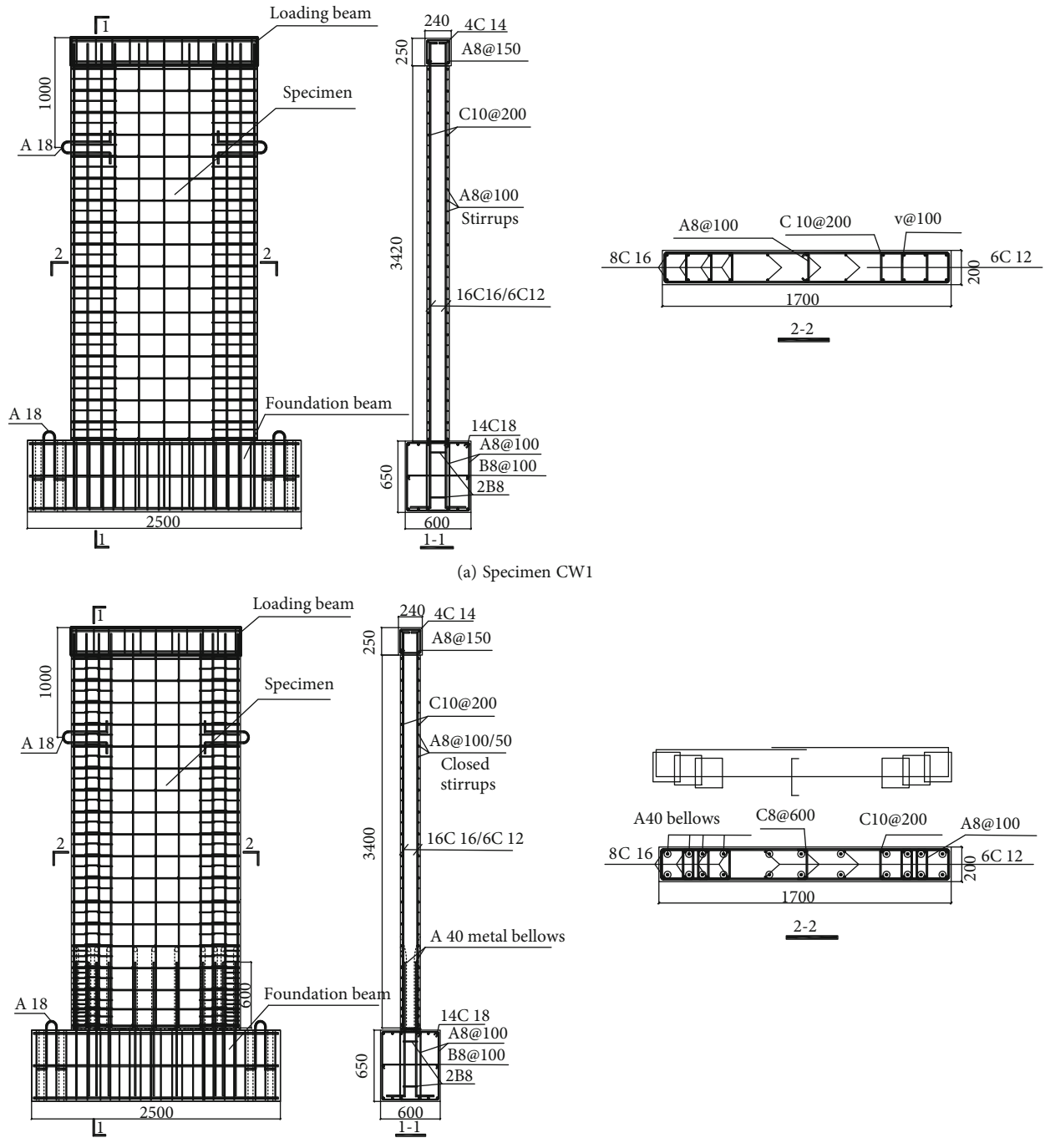

(a) Specimen CW1

(b) Specimen FW1 and FW2

Figure 1: Dimensions and reinforcement details of the test specimens.

uniformly loaded through the loading beam and distribution beam; the horizontal repeated load is applied through the 100 t electrohydraulic servo actuator (MTS); antilateral displacement devices are installed on both sides of the wall to avoid out-of-plane displacement. During the test, the vertical load is applied first, and the axial compression ratio is controlled to 0.1, and the calculated vertical load was 750 kN. The loading protocol was a hybrid load-displacement control as described in Figure 4. According to the Chinese Code Specification for Seismic test of Building JGJ/T 101-2015 [32], the graded loading procedure is as follows. In the initial stage of loading, each stage is increased by 50 kN; after loading to 100kN, each stage is increased by 40 kN. The cracking load is determined by the load value when the first horizontal crack or oblique crack of the specimen appears, and the loading is changed to every 20 kN level after loading to the

Table 1: Measurements of mechanical properties of concrete.

Concrete category	Test block number	Cubic compressive strength f_{cu} (MPa)	Weighted average compressive strength $f_{cu,ave}$ (MPa)
Cast-in situ shear wall concrete	A1	40.2	41.1
	A2	41.1	
	A3	41.9	
PC shear wall concrete	B1	40.8	41.9
	B2	42.1	
	B3	42.9	
Grouting material	C1	74.6	75.2
	C2	75.4	
	C3	75.6	

Table 2: Measurements of mechanical properties of steel.

Steel Type	Diameter (mm)	Average yield stress f_y (MPa)	Average ultimate stress f_u (MPa)	Elastic modulus E_s (GPa)	Elongation rate (%)
HPB300	8	443	647	207	11.8
HPB335	8	451	621	160	10.8
HPB400	10	429	552	152	17.4
HPB400	12	431	582	147	18.7
HPB400	14	458	638	136	19.7
HPB400	16	438	602	141	20.4
HPB400	18	551	780	169	21.3

Figure 2: Assembled specimens.

cracking load and continues to load to the calculated value of yield load, cycling once per level. Subsequently, displacement control is adopted for loading, and each level is cycled 3 times and loaded by integer multiples of the displacement value corresponding to the yield load.

3. Experimental Results and Discussion

3.1. Failure Process and Modes. A 10 cm × 10 cm grid was marked on the surface of the shear wall to accurately measure the location and shape of the cracks. The lines marked on the shear wall represent the crack direction of concrete in the specimen under reciprocating load; the crack distribution is shown in Figure 5.

3.1.1. CW1. For specimen CW1, horizontal cracks appeared on both sides of the specimen when it was loaded to 200 kN. In the process of loading up to 240 kN, the horizontal cracks gradually increased, and the crack width did not increase much. When it reached 320 kN, the specimen entered the yielding stage, and the interlayer displacement was 15 mm. After that, displacement control loading was adopted, and the seam developed obliquely when it was loaded to 30 mm, and the crack width increased faster,

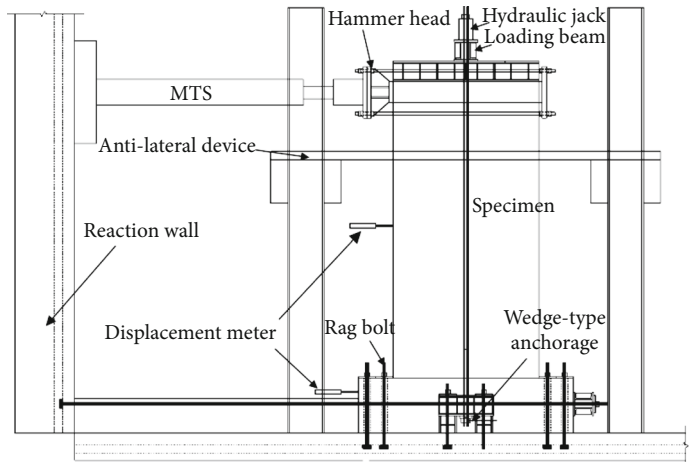

Figure 3: Test setup.

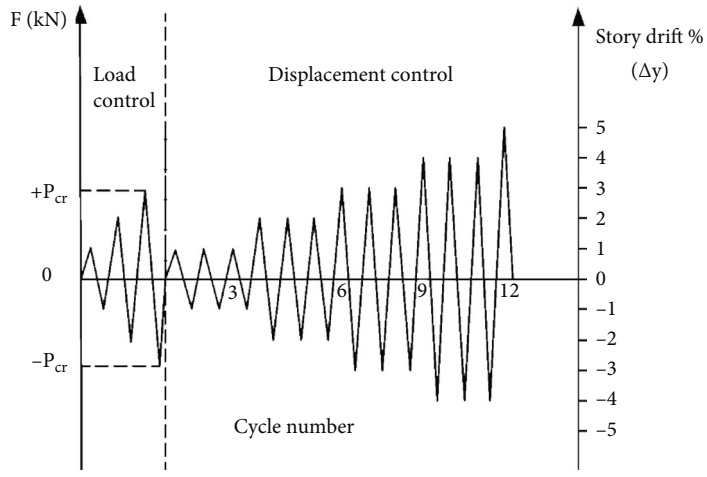

Figure 4: Loading protocol of the cyclic loading tests.

and the maximum crack width was 0.4 mm, as shown in Figure 6(a). When it was loaded to 45 mm, vertical cracks appeared on the concrete at the bottom edge of the specimen, and the crushing phenomenon began to appear, and there were basically no new cracks in the shear wall specimen as a whole and the maximum. When the loading was continued to 90 mm, the joint width increased, and the concrete at the bottom edge of the wall was seriously dislodged. When the displacement reaches 105 mm, the concrete at the corner of the specimen is crushed and the reinforcement is exposed, and the damage pattern is shown in Figure 6(a).

3.1.2. FW1 and FW2. The damage process and crack distribution of specimens FW1 and FW2 are basically the same as those of cast-in-place specimen CW1, both of which are bending shear damage, and the cracks are in the shape of "X" when the damage occurs, as shown in Figures 5(b) and 5(c). When the force is loaded to the cracking stage, the horizontal cracks develop slowly from both sides of the wall to the middle of the wall. When the force is loaded to the yielding stage, the horizontal crack in the compression area of the specimen expands diagonally and extends. When the loading was continued to the ultimate stage, the horizontal joints of both assembled specimens were cracked, and the concrete was exposed at the metal bellows after the damage. The assembled specimens were subjected to horizontal rotation on the seated slurry layer due to the restriction of the MTS antilateral shift device, and the damage pattern of FW1 was caused by the failure of displacement control loading due to the toppling of the antilateral shift device, as shown in Figure 6(b). The specimen FW2 was damaged prematurely due to the additional horizontal displacement caused by the horizontal rotation, resulting in the premature disconnection of the vertical reinforcement, and the damage pattern is shown in Figure 6(c).

3.2. Hysteresis Performance and Load-Carrying Capacity. The hysteresis curves of each specimen are shown in Figure 7. Contrast analysis shows that the specimens are basically in elastic state before cracking, and when loaded to cracking without yielding, the residual deformation is

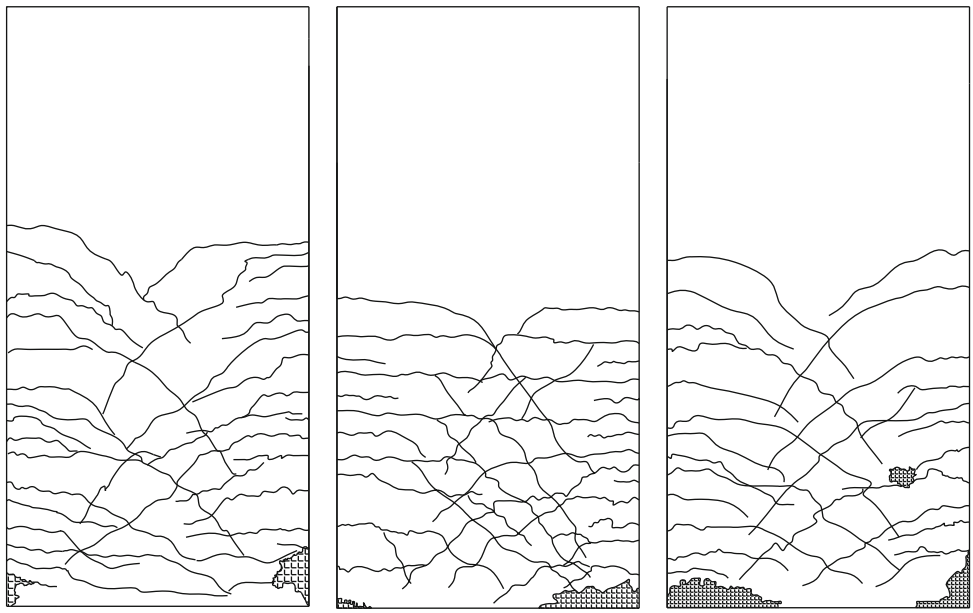

Figure 5: Crack distributions on specimens.

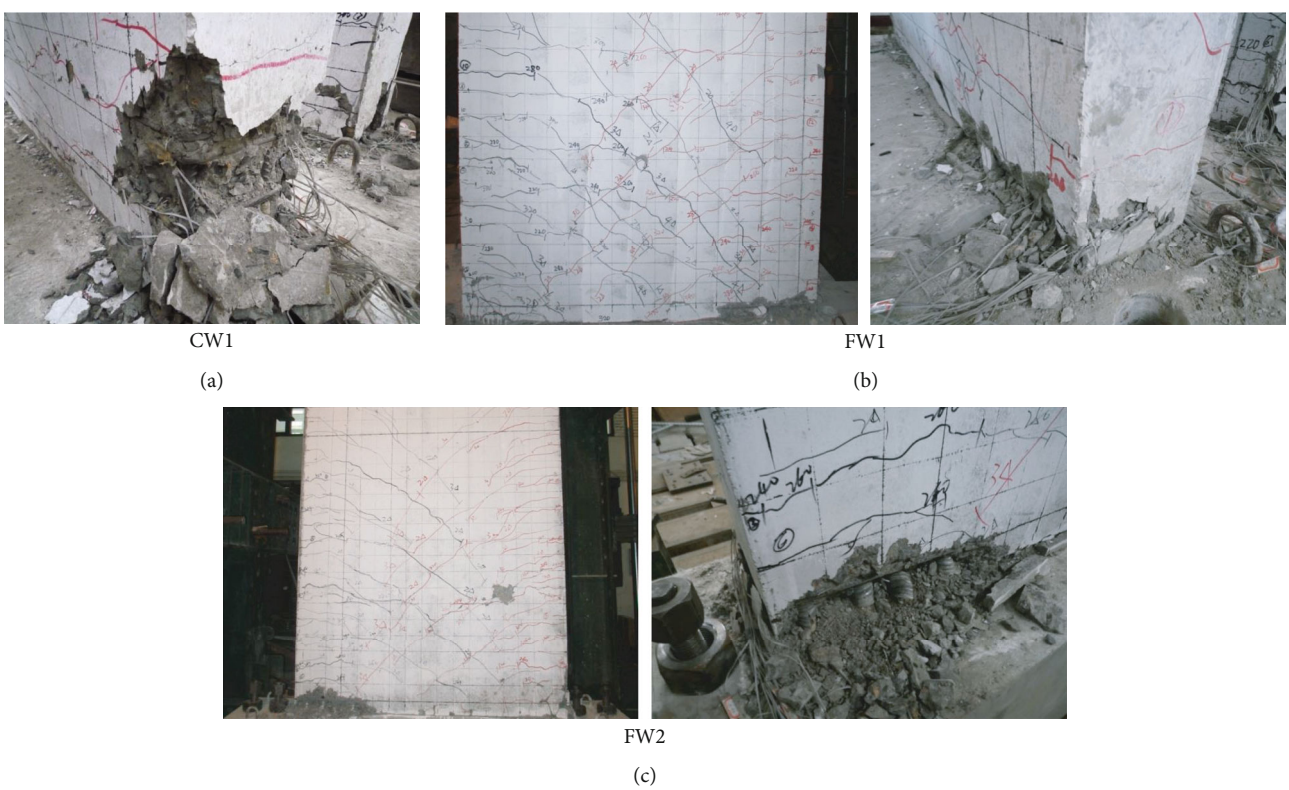

Figure 6: Cracking and damage of the specimens.

smaller and the hysteresis loop area is smaller, and the PC shear wall specimen has a certain degree of decrease in overall stiffness due to cracks at the bottom horizontal joints. After yielding, the overall hysteresis curve tilts toward the displacement axis, and the hysteresis loop gradually appears fuller with good energy dissipation capacity. At the ultimate

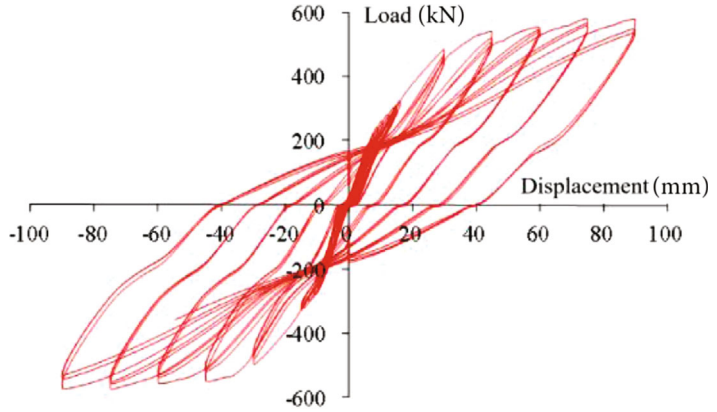

(a) FW1

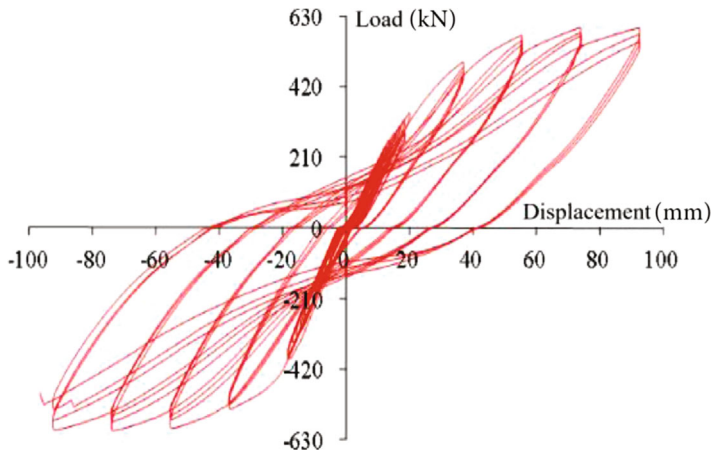

(b) FW1

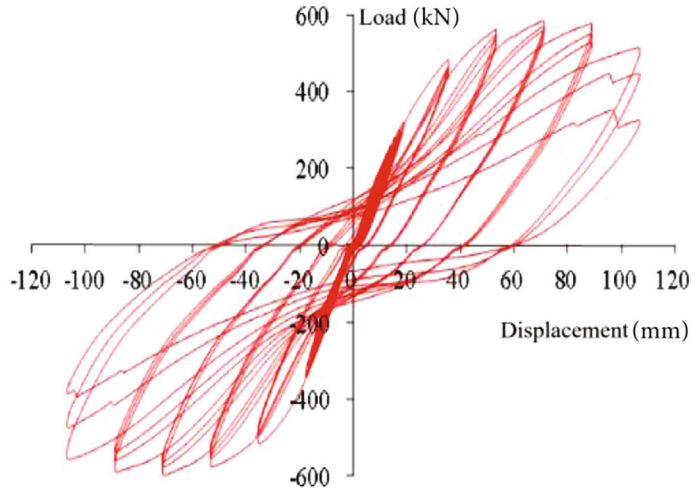

(c) FW2

Figure 7: Hysteretic curves.

state, the hysteresis curves of specimens FW1 and FW2 have a certain pinching phenomenon, which is due to the slip at the horizontal joints of the PC specimens.

The skeleton curves of each specimen are shown in Figure 8. After reaching the limit state, it can be found that the shapes of the three curves are relatively similar, except for specimen FW2, where the load capacity decreases more rapidly due to the torsion of the specimen caused by the limitation of the MTS capacity of the loading equipment, and all other specimens have a slow decrease in load capacity. Table 3 shows the load and displacement values of each specimen characteristic point, where the yield load is determined by Park's method [33]. As can be seen from Table 3, the cracking displacements of PC specimens FW1 and FW2

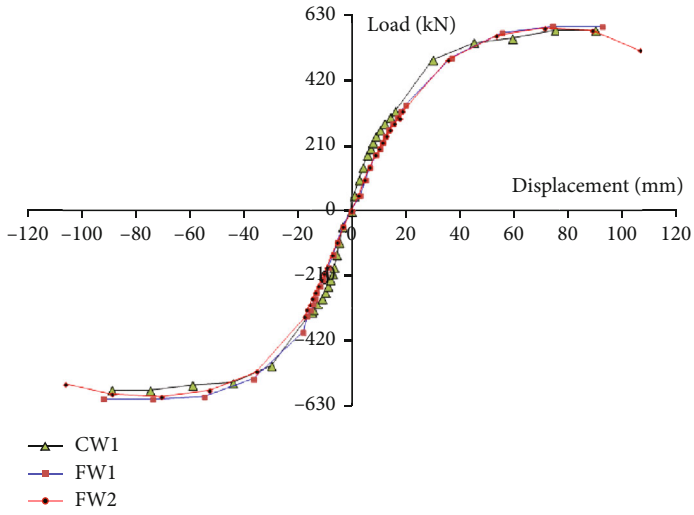

Figure 8: Skeleton curves.

Table 3: Characteristic value of specimens.

Specimen	Cracking		Yield			Ultimate load			Ductility factor
	P_C (kN)	$\triangle c$ (mm)	P_y (kN)	$\triangle y$ (mm)	θ_y	P_u (kN)	$\triangle p$ (mm)	θ_p	μ
CW1	200	6.95	320	15	1/227	580	90	1/38	6
FW1	200	10	340	18.5	1/184	605	92.5	1/37	5
FW2	200	10.1	320	17.8	1/191	598	106.8	1/32	6

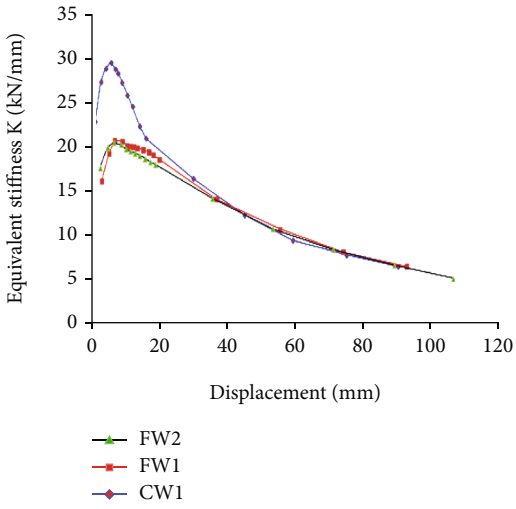

Figure 9: Stiffness degradation.

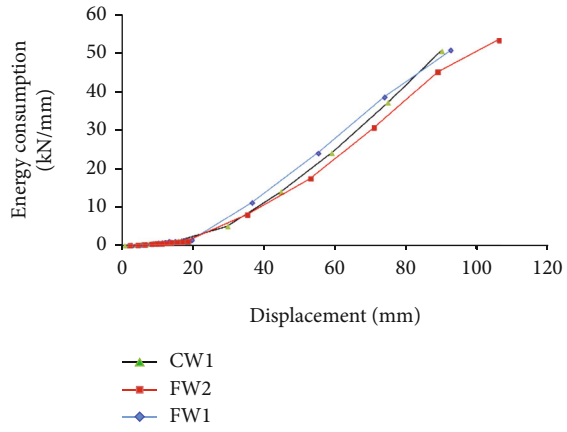

Figure 10: Cumulative energy dissipation of specimens.

increased by 43.9% and 45.3%, respectively, compared with cast-in-place specimen CW1, which is due to the restraint of the vertical reinforcement of the edge members of the PC specimens by using buckled closed stirrups, which has a strengthening effect on the horizontal joints of the wall. The peak loads of PC specimens FW1 and FW2 are not much different or slightly improved compared with cast-in-place specimen CW1, and the overall performance is comparable to that of cast-in-place specimens in terms of bearing capacity.

3.3. Ductility. Table 3 lists the displacement angle and displacement ductility coefficient of each specimen at each characteristic point, the displacement angle $\theta = \triangle/H$, where H is the height of the wall, and the displacement ductility coefficient μ is the ratio of yield displacement to ultimate displacement. As can be seen from the Table 3, the deformation values of PC specimens FW1 and FW2 at each stage are similar to those of cast-in-place specimen CW1, achieving

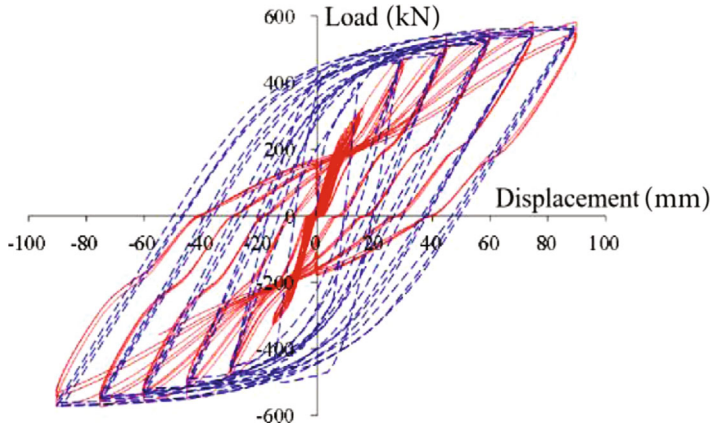

(a) CW1

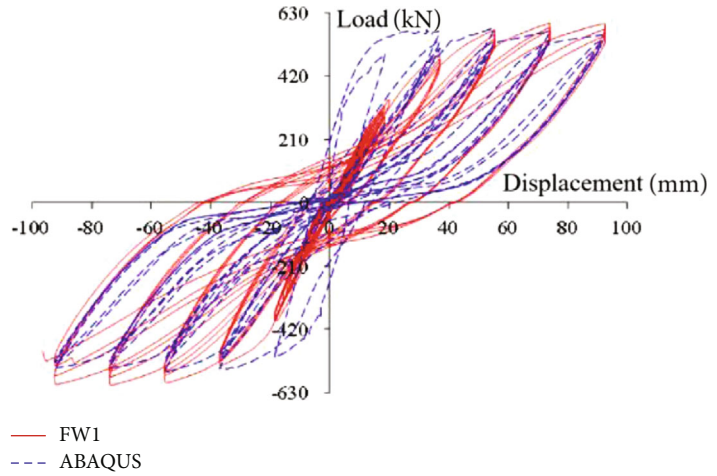

(b) FW1

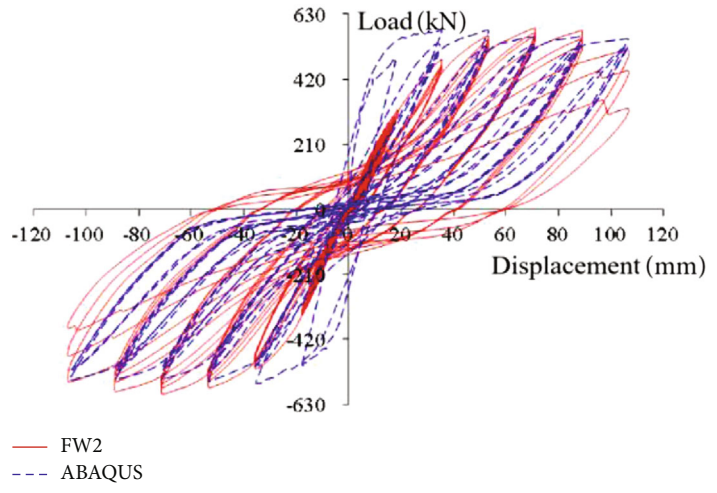

(c) FW2

Figure 11: Specimen hysteresis curve comparison chart.

the effect of "equivalent to cast-in-place." The ultimate displacement angle is slightly larger than that of the cast-in-place specimen CW1 and is greater than the elastic-plastic interstory displacement angle limit of 1/120 as stipulated in the Code for Seismic Design of Buildings (GB50010-2010) [30], which indicates that the deformation capacity of the

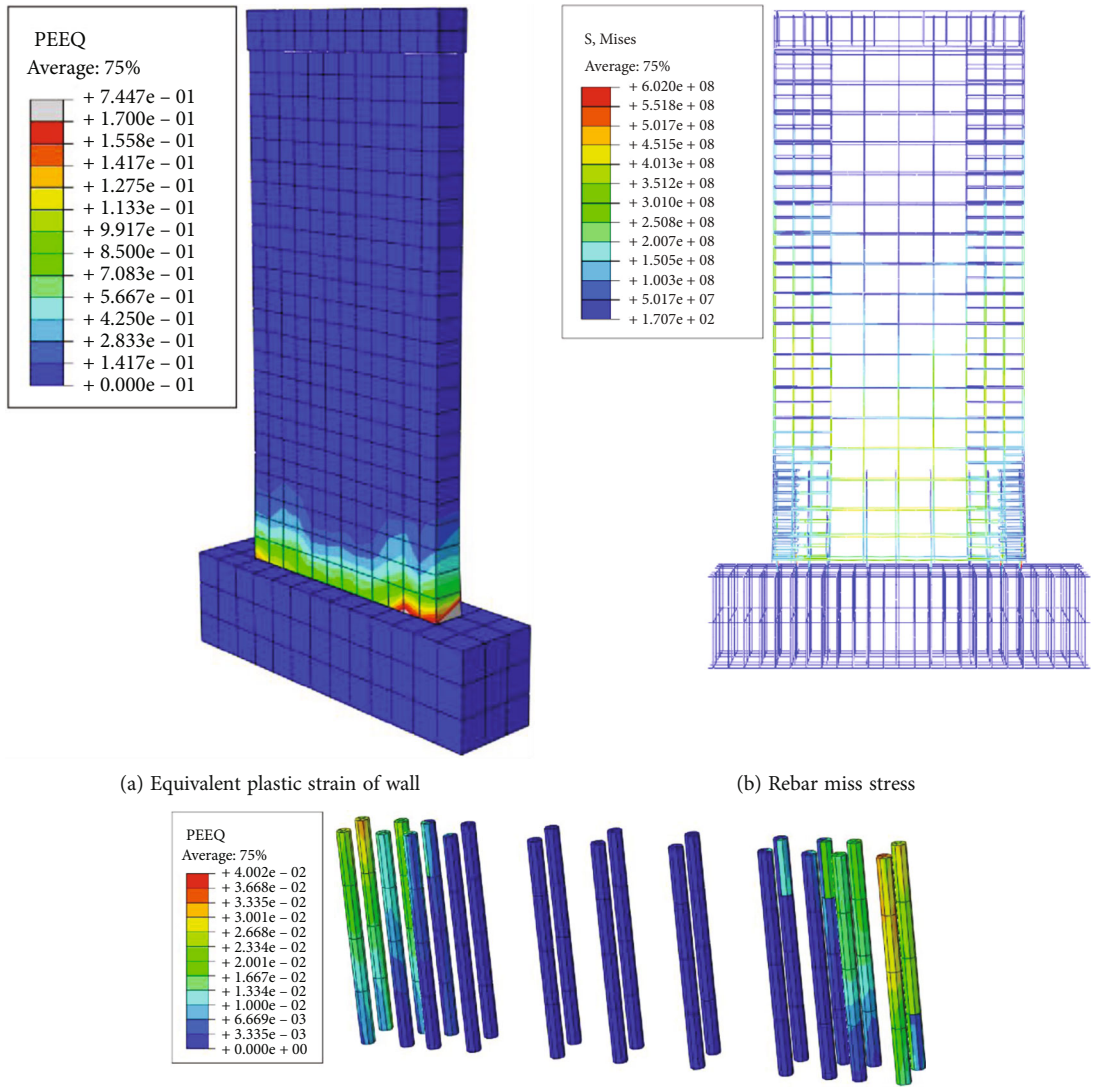

(a) Equivalent plastic strain of wall

(b) Rebar miss stress

(c) Equivalent plastic strain of grout

Figure 12: FEA stress results of specimen FW1.

vertical reinforcement lap assembly shear wall specimen is better. The displacement ductility coefficients of all specimens are similar and greater than 5, indicating that the closed stirrup reinforcement has a significant restraining effect on the concrete of the PC wall edge members and can improve the integrity of the PC shear wall with horizontal joints.

3.4. Stiffness Degradation. During the loading process, the stiffness degradation of each specimen is shown in Figure 9. As can be seen from Figure 9, the equivalent stiffness of the cast-in-place specimen is larger during the force loading stage, and the initial stiffness of the two assembled specimens is lower than that of the cast-in-place specimen due to the cracking at the horizontal joints. With the increase of displacement, the stiffness of each specimen gradually degrades, and the degradation rate of cast-in-place specimen is faster before yielding and gradually slows down after yielding, and the stiffness degradation curve of each specimen gradually approaches after yielding.

3.5. Energy Dissipation. The energy dissipation capacity of the specimen is measured by the area enclosed by the hysteresis curve. Figure 10 shows the energy dissipation curve of each specimen; the curves of each specimen basically overlap at the initial stage of loading. With the increase of horizontal displacement, the energy consumption of each specimen increases continuously and increases rapidly. At the same displacement, the cumulative energy dissipation of PC specimen FW1 is larger than that of cast-in-place specimen CW1, and the cumulative energy dissipation of PC specimen FW2 is lower due to torsion during the displacement loading control stage. However, when the specimens were loaded to the ultimate state, the final cumulative values of both PC shear walls FW1 and FW2 were slightly larger than those

Table 4: Design parameters of each finite element piece.

Specimen	Axial compression ratio	Aspect ratio	Concrete strength	Vertical connection diameter of steel bar (mm)
FW1	0.1	2.01	C35	16
FW3	0.2	2.01	C35	16
FW4	0.3	2.01	C35	16
FW5	0.4	2.01	C35	16
FW6	0.5	2.01	C35	16
FW7	0.1	1.42	C35	16
FW8	0.1	1.6	C35	16
FW9	0.1	1.78	C35	16
FW10	0.1	2.25	C35	16
FW11	0.1	2.42	C35	16
FW12	0.1	2.01	C40	16
FW13	0.1	2.01	C45	16
FW14	0.1	2.01	C50	16
FW15	0.1	2.01	C35	12
FW16	0.1	2.01	C35	14
FW17	0.1	2.01	C35	18

of cast-in-place specimen CW1, reflecting the advantages of the assembled shear walls with built-in metal bellows and closed stirrup restraint.

4. Modeling

4.1. Model Building. Three specimens were simulated by ABAQUS finite element software, with three-dimensional solid units (C3D8R) for both concrete and grout and line units (T3D2) for reinforcement. In addition, for the convenience of modeling and the metal bellows and sit grout layer thickness, wall performance is less affected, and the part where it is located is replaced with concrete material. The plastic damage material model [34], which comes with the software, is used for the concrete principal structure relationship, the Mander model [35] is used for the grout compressive principal structure, the tensile principal structure is simplified to the high-strength concrete principal structure model, and the reinforcement principal structure model is often used as a reinforced bifold model with the material parameters taken from the measured values. The new and old concrete interface bonding problem existing in horizontal cracks is simulated by setting the cohesive connection that comes with the program to simulate the slip relationship between the joints.

The mesh generation is crucial in the establishment of the finite element model; the mesh size of each part of the precast shear wall specimen is determined through a large number of trial calculations. The unit size of the reinforcement in the wall is 100 mm, and the unit size of the shear wall, and the grouting material is 140 mm. For the nonimportant parts such as the loading beam and the base, the unit sizes are 150 mm and 200 mm.

4.2. Model Validation. A comparison of the finite element analysis and the hysteresis curve obtained from the test is shown in Figure 11. As can be seen from the Figure 11, the hysteresis curves of assembly specimen FW1 and FW2 roughly match the test, and the hysteresis curve of the finite element model of cast-in-place specimen CW1 is fuller than the measured curve, probably because the cast-in-place specimen produced a larger bond slip between the reinforcement and concrete during the experiment, which was not considered during the numerical simulation. The simulated value of the ultimate bearing capacity of each specimen is closer to the experimental value, and the maximum error is controlled within 6%. In addition, before the specimen yielded, the specimen load obtained by FEA was significantly higher than the experimental value, which may be due to the bond slip between the reinforcement and concrete during the actual loading process, and the defects in the specimen fabrication. After the specimen yielded, the peak load obtained from the FEA was slightly lower than the experimental value, which was due to the fact that the damage plasticity model used in the FEA was more idealized and could not fully simulate the complex force situation at the later stage of loading.

Since this paper studies the construction of improved assembled shear walls, the size and reinforcement of the two specimens FW1 and FW2 are the same; for the convenience of comparison and to save space, only the calculation results of the corresponding model of specimen FW1 are given here as shown in Figure 12; the unit of stress cloud map is Pa and the unit of strain cloud map is m. From Figure 12, it can be found that the plastic strains in the concrete of the assembled specimens are concentrated at the corners of the two ends of the shear wall, and the grout plastic strains are concentrated at the edge members on both

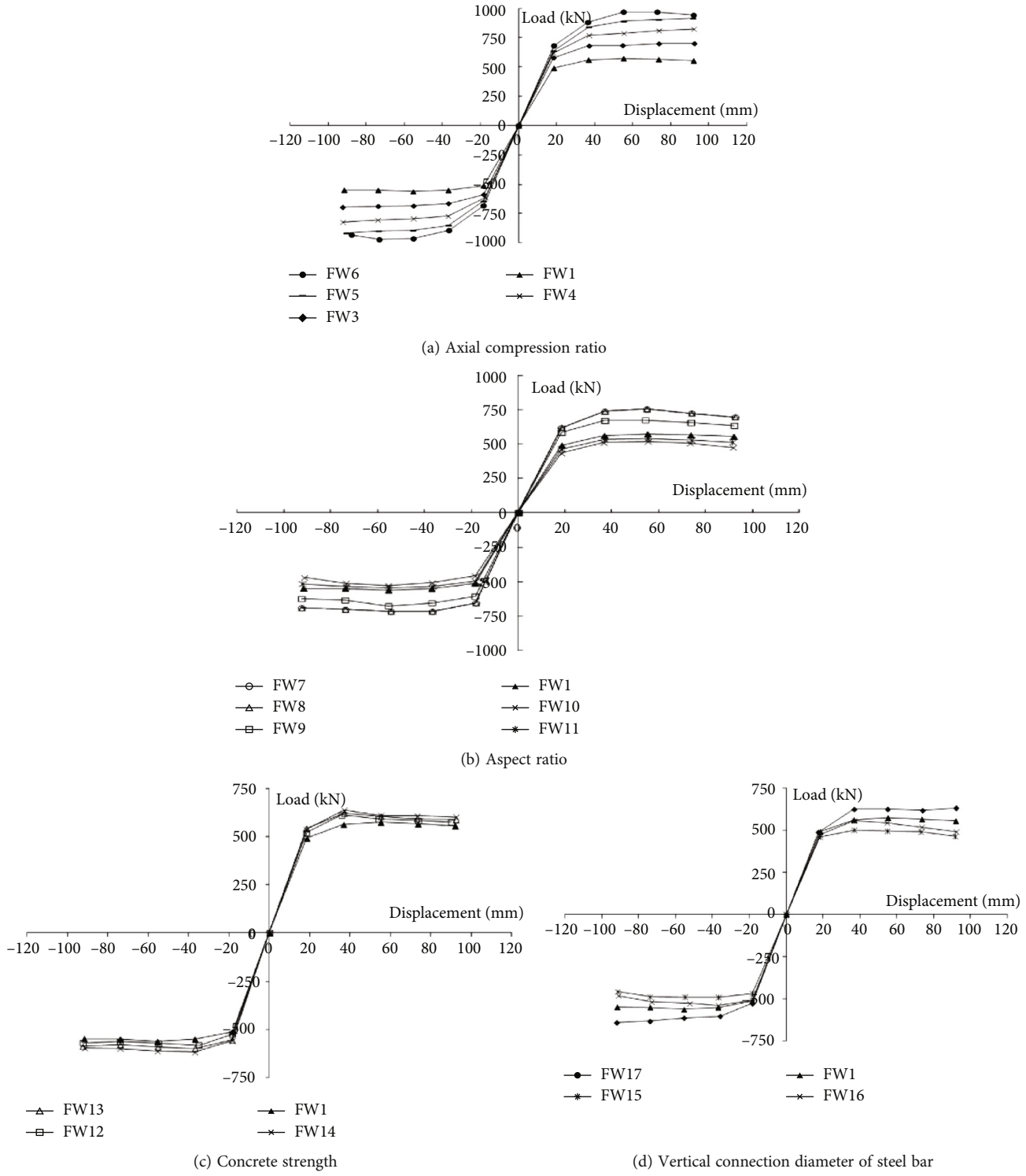

Figure 13: Load-displacement curve of each parameter.

sides of the shear wall, and the overall strain level is low. The maximum stresses in the reinforcement are distributed at the vertical connection reinforcement at the bottom of the two ends of the shear wall, indicating that the grout-anchor connection method with buckle-closed stirrup restraint can effectively transfer the longitudinal reinforcement stresses.

5. Parameter Analyses

According to the characteristics of the connection structure of the assembled shear wall, the range of analysis parameters was expanded, and the finite element model established in Section 3.1 was used to further investigate the effects of axial compression ratio, height-to-width

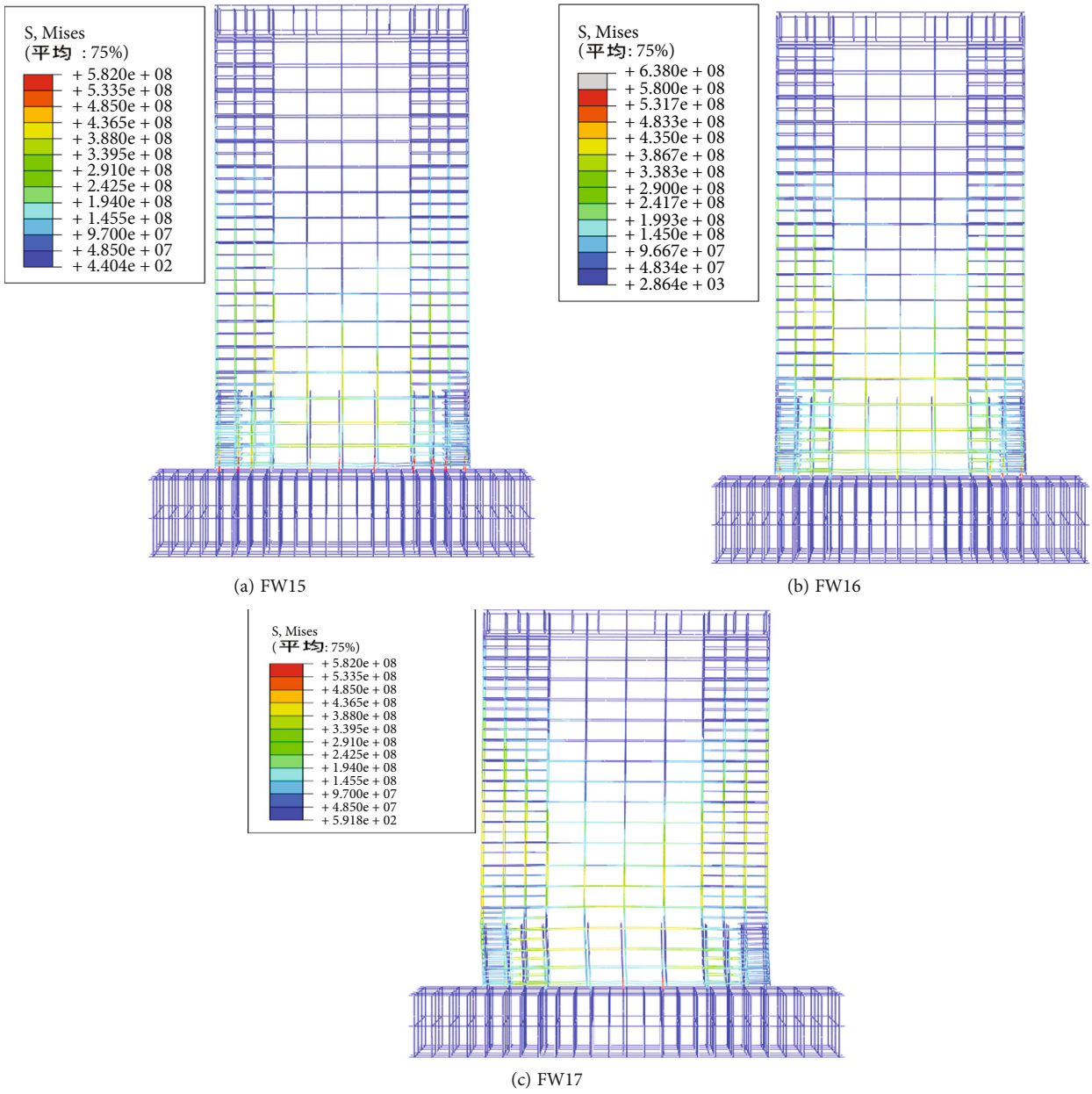

(a) FW15

(b) FW16

(c) FW17

Figure 14: Reinforced stress cloud map for specimens.

ratio, longitudinal connection reinforcement diameter, and concrete strength on the seismic performance of the PC shear wall with vertical reinforcement slurry-anchored lap, with the model parameters shown in Table 4. The load-displacement curves obtained from the finite element analysis of the vertical reinforcement slurry-anchored lap PC shear walls with different parameters are shown in Figure 13.

5.1. Axial Compression Ratio. Since the axial compression ratio limit for seismic shear walls of medium and high intensities is 0.5, the effects of five converted axial compression ratio cases with axial compression ratios of 0.1 to 0.5 on horizontal jointed PC shear walls are considered. From Figure 13(a), it can be seen that the increase of the axial compression ratio will significantly improve the stiffness and bearing capacity of this PC shear wall model. When the axial compression ratio is 0.1~0.4, with the increase of axial compression ratio, the curve bending is lagged and the bearing capacity decreases gradually and smoothly, but when the axial compression ratio reaches 0.5, the curve bending is advanced and the bearing capacity decreases faster, which will be unfavorable to the ductility and energy dissipation of the wall.

5.2. Aspect Ratio. The available research data show that the height-to-width ratio of shear walls has a large influence on the seismic performance of this structure, so the finite element model of shear walls with height-to-width ratios of

2.01 to 2.42 is designed. From Figure 13(b), it can be seen that the peak load of the model gradually decreases as the aspect ratio increases, and the peak load decreases most significantly when the axial compression ratio increases from 1.78 to 2.01. For the shear wall model with the aspect ratio of 1.42 to 1.78, the load-displacement curve obtained has an obvious decreasing segment, which may be due to the shear damage of the wall; for the shear wall model with the aspect ratio of 2.01 to 2.42, the load-displacement curve decreases slowly, which indicates that the ductility of the model is good. Therefore, it is recommended that the height-to-width ratio of this shear wall is not less than 2.0.

5.3. Concrete Strength. To study the effects of various concrete strengths on the seismic performance of PC shear walls, C35, C40, C45, and C50 concrete strength grade model specimens were selected for analysis in the simulation process. From Figure 13(c), it can be seen that the peak load of the PC shear wall model gradually increases with the increase of concrete strength, and the increase of bearing capacity gradually slows down. When the concrete strength is C50, the decreasing section of the load-displacement curve of the specimen after reaching the peak load is the most drastic, and the model shows the characteristics of brittle damage. In summary, it is recommended that the concrete strength used in this PC shear wall should not be higher than C45.

5.4. Vertical Connection Diameter of Steel Bar. The horizontal joint of PC shear wall is mainly to solve the problem of vertical reinforcement connection of shear wall. On the basis of the original 16 mm vertical connection reinforcement diameter PC shear wall model, three models of 12 mm, 14 mm, and 18 mm vertical connection reinforcement diameters are added to consider the influence of vertical connection reinforcement diameter on this PC shear wall. From Figure 13(d), it can be seen that the size of the vertical connection reinforcement diameter has a more obvious effect on the load-displacement curve, which shows that with the increase of the vertical connection reinforcement diameter, the model stiffness and bearing capacity of the shear wall model are significantly increased, and the bearing capacity decreases gradually and smoothly when the model reaches the limit stage. The stress cloud map of each specimen is shown in Figure 14, when the diameter of vertical connection reinforcement is 14 mm, the vertical connection steel bar was finally pulled out, resulting in low bearing capacity of the specimen after yield, which was manifested as shear failure and was not suitable for the structural design, so it is suggested that the diameter of vertical connection reinforcement of this PC shear wall is not less than 16 mm.

6. Conclusions

The connection of PC shear walls with vertical reinforced grouting anchors restrained by buckling closed stirrups was investigated. The wall specimens are subjected to low-cycle repeated load tests and finite element simulation analysis; the main conclusion can be summarized as follows:

(1) The failure mode of PC shear wall restrained by buckle-closed stirrups in seismic test is close to that of cast-in-place shear wall, and all of them are flexural-shear failure. The weakest part of PC shear wall restrained by buckle-closed stirrups is still horizontal joint, but there is no obvious bond failure in the slurry-anchored connection at the horizontal joint. The buckle-closed stirrups have a good constraint effect on the bottom of PC shear wall

(2) The new slurry-anchored lap PC shear wall specimens have positive seismic performance, stronger bearing capacity and displacement ductility performance than cast-in-place shear walls, and similar energy dissipation capacity as cast-in-place shear walls but lower initial stiffness than cast-in-place shear walls. The slurry-anchored connection with buckle-type-closed stirrup restraint can effectively transfer the stress of reinforcement, so that it can achieve the effect of "equivalent to cast-in-place," which is worth further research and application

(3) The bearing capacity and deformation performance of the new PC shear wall finite element model are in good agreement with the test results. Within a certain range, increasing the axial compression ratio, the diameter of vertical connecting steel bars, and the strength of concrete can improve the stiffness and bearing capacity of the shear wall structure; with the increase of the aspect ratio, the bearing capacity of this type of PC shear wall decreases, as PC shear wall stiffness degradation slows, ductility and energy dissipation capacity increase

Data Availability

Some or all data, models, or code that support the findings of this study are available from the corresponding author upon reasonable request.

Conflicts of Interest

The authors declare that they have no conflicts of interest.

References

[1] Y. C. Wu, L. P. Sheng, and W. J. Zhao, "Research and development status of grouted splice sleeve in precast concrete structure," *E3S Web of Conferences*, vol. 38, pp. 30–34, 2018.

[2] X. W. Xiao, Z. W. Cao, X. Liu, and X. D. Liao, "Status, problems and countermeasures of prefabricated buildings in China," *Build. Struct.*, vol. 19, 2019.

[3] A. Biswal, A. M. Prasad, and A. K. Sengupta, "Study of shear behavior of grouted vertical joints between precast concrete wall panels under direct shear loading," *Structural Concrete*, vol. 20, no. 2, pp. 564–582, 2019.

[4] S.-D. Shen, P. Pan, Q.-S. Miao, W.-F. Li, and R.-H. Gong, "Test and analysis of reinforced concrete (RC) precast shear wall assembled using steel shear key (SSK)," *Earthquake Engineering & Structural Dynamics*, vol. 48, no. 14, pp. 1595–1612, 2019.

[5] C. A. Bei, C. A. Yuan, and B. Dtwl, "Experiment and numerical study of a new bolted steel plate horizontal joints for precast concrete shear wall structures," *Structure*, vol. 32, pp. 760–777, 2021.

[6] X. Chong, L. Xie, and X. Ye, "Experimental study on the seismic performance of superimposed RC shear walls with enhanced horizontal joints," *Journal of Earthquake Engineering*, vol. 23, no. 1-2, pp. 1–17, 2019.

[7] J. Sun, H. Qiu, and Y. Lu, "Experimental study and associated numerical simulation of horizontally connected precast shear wall assembly," *Structural Design of Tall and Special Buildings*, vol. 25, no. 13, pp. 659–678, 2016.

[8] J. Sun, H. Qiu, Y. Yang, and B. Lu, "Experimental and analytical studies on the deformability of a precast RC shear wall involving bolted connections," *Science China Technological Sciences*, vol. 58, no. 8, pp. 1439–1448, 2015.

[9] J. Sun, H. Qiu, and B. Lu, "Experimental validation of horizontal joints in an innovative totally precast shear wall system," *J Southeast Univ (English Ed)*, vol. 31, pp. 124–129, 2015.

[10] L. Wanrun, "Experimental study of seismic performance of precast shear wall with a new bolt-plate connection joint," *Structure*, vol. 34, pp. 3818–3833, 2021.

[11] H. A. D. Samith Buddika and A. C. Wijeyewickrema, "Seismic shear forces in post-tensioned hybrid precast concrete walls," *Journal of Structural Engineering*, vol. 144, no. 7, 2018.

[12] C.-f. Sun, S.-t. Liang, X.-j. Zhu et al., "Experimental study and numerical simulation of precast shear wall with rabbet-unbonded horizontal connection," *International Journal of Concrete Structures and Materials*, vol. 14, no. 1, 2020.

[13] S. Singhal, A. Chourasia, and J. Parashar, "Anchorage behaviour of headed bars as connection system for precast reinforced concrete structural components," *Structure*, vol. 27, pp. 1405–1418, 2020.

[14] T. Holden, J. Restrepo, and J. B. Mander, "Seismic performance of precast reinforced and prestressed concrete walls," *Journal of Structural Engineering*, vol. 129, no. 3, pp. 286–296, 2003.

[15] M. Wu, X. Liu, H. Liu, and X. Du, "Seismic performance of precast short-leg shear wall using a grouting sleeve connection," *Engineering Structures*, vol. 208, p. 110338, 2020.

[16] Q. Zhi, L. Kang, L. Jia, J. Xiong, and Z. Guo, "Seismic performance of precast shear walls prestressed via post-tensioned high strength bars placed inside grouted corrugated pipes," *Engineering Structures*, vol. 237, no. 7, article 112153, 2021.

[17] S. Sritharan, S. Aaleti, R. S. Henry, K. Y. Liu, and K. C. Tsai, "Precast concrete wall with end columns (PreWEC) for earthquake resistant design," *Earthquake Engineering and Structural Dynamics*, vol. 44, no. 12, pp. 2075–2092, 2015.

[18] Q. Luo, X. Chen, M. Gao, Z. Li, Z. Zhang, and D. Zhou, "Simulating the near-fault large velocity pulses of the Chi-Chi (Mw7.6) earthquake with kinematic model," *Journal of Seismology*, vol. 23, no. 1, pp. 25–38, 2019.

[19] Q. Luo, F. Dai, Y. Liu, and X. Chen, "Simulating the near-field pulse-like ground motions of the Imperial Valley, California, earthquake," *Soil Dynamics and Earthquake Engineering*, vol. 138, article 106347, 2020.

[20] Q. Luo, F. Dai, Y. Liu, M. Gao, Z. Li, and R. Jiang, "Seismic performance assessment of velocity pulse-like ground motions under near-field earthquakes," *Rock Mechanics and Rock Engineering*, vol. 54, no. 8, pp. 3799–3816, 2021.

[21] J. Li, Y. Wang, Z. Lu, and B. Xia, "Shaking table test and numerical simulation of a superimposed reinforced concrete shear wall structure," *The Structural Design of Tall and Special Buildings*, vol. 27, no. 2, 2018.

[22] W. C. Xue, Y. Li, L. Cai, and X. Hu, "Seismic performance of precast concrete composite shear walls with multiple boundary elements," *Journal of Earthquake and Tsunami*, vol. 13, p. 1940006, 2019.

[23] JGJ/T 430-2018, *Technical Standard for Precast Reinforced Concrete Shear Wall Structure Assembled by Anchoring Closed Loop Reinforcement. MOHURD Ministry of Housing and Urban-Rural Development of the People's Republic of China*, China Architecture anddd Building Press, Beijing, China, 2018.

[24] Aci, *318-14. Building Code Requirements for Structural Concrete and Commentary. ACI Committee 318*, American Concrete Institute, Farmington Hills, MI, 2014.

[25] EN 1992-1-1: 2004, *Eurocode 2: Design of concrete structures-Part 1-1: General rules and rules for buildings*, CEN (European Committee for Standardization), 2004.

[26] DIN 1045-1, *Plain, Reinforced and Prestressed Concrete Structures, Part 1: Design and construction*, ISO (International Organization for Standardization), 2001.

[27] J. Jiang, J. Luo, W. Xue, X. Hu, and D. Qin, "Seismic performance of precast concrete double skin shear walls with different vertical connection types," *Engineering Structures*, vol. 245, 2021.

[28] A. L. Jiao, P. Zhang, Y. H. Li, and X. D. Zhi, "Tests on seismic behavior of pre-cast shear walls with annular closed reinforcements," *J Build Struct*, vol. 36, 2015.

[29] N. Rossley, F. N. A. A. Aziz, and H. C. Chew, "Behavior of precast walls connection subjected to shear load," *Journal of Engineering Science and Technology*, pp. 142–150, 2014.

[30] *GB50010-2010, Code for Seismic Design of Buildings*, China Building Industry Press, Beijing, 2016.

[31] *GB/T 51231-2016, Technical Code for Assembled Buildings with Concrete Structure*, China Building Industry Press, Beijing, 2016.

[32] JGJ/T 101-2015, *Specification for Seismic test of Building*, China Building Industry Press, Beijing, 2015.

[33] R. Park, "Evaluation of ductility of structures and structural assemblages from laboratory testing," *Bulletin of the New Zealand National Society for Earthquake Engineering*, vol. 22, no. 3, pp. 155–166, 1989.

[34] DASSAULT SYSTEMES, *ABAQUS Analysis User's Manual Version 2016*, Waltham, MA, 2016.

[35] M. A. N. D. E. R. Jab and P. R. I. E. S. T. L. E. Y. Mjn, "Theoretical stress-strain model for confined concrete," *Journal of Structural Engineering*, vol. 114, no. 8, pp. 1804–1826, 1988.